J|A|C|S
ARTICLES
Published on Web 04/13/2004

Origin, Nature, and Fate of the Fluorescent State of the Green Fluorescent Protein Chromophore at the CASPT2//CASSCF Resolution

María Elena Martin,[†] Fabrizia Negri,[§] and Massimo Olivucci*[,†,‡]

Contribution from the Dipartimento di Chimica, Università di Siena, via Aldo Moro I-53100 Siena, Italy, Studio dei Sistemi Complessi, Via Tommaso Pendola 37, Siena I-53100, Italy, and Dipartimento di Chimica "G. Ciamician", Università di Bologna, via Selmi, 2, I-40100, Bologna, Italy

Received July 15, 2003; E-mail: olivucci@unisi.it

Abstract: Ab initio CASPT2//CASSCF relaxation path computations are employed to determine the intrinsic (e.g., in vacuo) mechanism underlying the rise and decay of the luminescence of the anionic form of the green fluorescent protein (GFP) fluorophore. Production and decay of the fluorescent state occur via a two-mode reaction coordinate. Relaxation along the first (totally symmetric) mode leads to production of the fluorescent state that corresponds to a planar species. The second (out-of-plane) mode controls the fluorescent state decay and mainly corresponds to a barrierless twisting of the fluorophore phenyl moiety. While a "space-saving" hula-twist conical intersection decay channel is found to lie only 5 kcal mol^{-1} above the fluorescent state, the direct involvement of a hula-twist deformation in the decay is not supported by our data. The above results indicate that the ultrafast fluorescence decay observed for the GFP chromophore in solution is likely to have an intrinsic origin. The possible effects of the GFP protein cavity on the fluorescence lifetime of the investigated chromophore model are discussed.

1. Introduction

The green fluorescence protein (GFP) constitutes the final emitter in the bioluminescence reaction of the jellyfish *Aequorea victoria*.[1,2] Spectroscopic and structural studies have established that the fluorophore of GFP (i.e., the protein luminescent prosthetic group) corresponds to a derivative of 5-(4′-hydroxybenzylidene)-3,5-dihydroimidazole-4-one.[3] More specifically, the fluorescence has been attributed to an anionic form of the fluorophore (see structure **1**) featuring an ionized 4-hydroxyl group.[4,5]

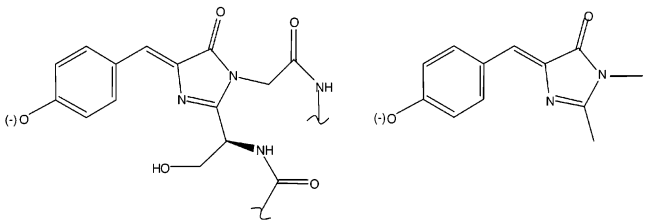

1 2

The fluorescence activity of **1** depends on the molecular environment. For instance, while wild-type GFP is strongly fluorescent, upon denaturation the fluorescence is lost and it is recovered only after reconstitution of the wild-type structure or cooling of the denaturated structure at 77 K. The investigation of the synthetic fluorophore derivative **2**,[6,7] as well as of other synthetic analogues of **1**,[5,8] has established that the environment dependent fluorescence of GFP can be related to the behavior of its fluorophore. In fact, while no room-temperature fluorescence can be detected for **2** in ethanol solution, this species fluoresces when confined in a cold (77 K) ethanol matrix.[5,7] This suggests that the fluorescent state (**FS**) of the GFP fluorophore undergoes a barrierless (or nearly barrierless) deactivation in solution but has a long lifetime when confined in a cold or properly designed molecular cavity. The fact that wild-type GFP is strongly fluorescent even at room temperature can thus be associated to the existence of an excited-state barrier because of specific electronic or steric effects of the protein cavity structure.

Recent time-resolved spectroscopy studies by the group of Meech[9] have provided direct evidence for the existence of a fully efficient fluorescence deactivation channel in **2**. Indeed, these authors have shown that in methanol, propanol, and decanol solution 90−60% of the fluorescence of this species

[†] Università di Siena.
[‡] Studio dei Sistemi Complessi.
[§] Università di Bologna.

(1) Davenport, D.; Nicol, J. A. C. *Proc. R. Soc. London, Ser. B* **1955**, *144*, 399.
(2) Harvey, E. N. *Biol. Bull.* **1921**, *41*, 280.
(3) Shimomura, O. *FEBS Lett.* **1979**, *104*, 220−222.
(4) Chattoraj, M.; King, B. A.; Bublitz, G. U.; Boxer, S. G. *Proc. Natl. Acad. Sci. U.S.A.* **1996**, *93*, 8362.
(5) Niwa, H.; Inouye, S.; Hirano, R.; Matsuno, T.; Kojima, S.; Kubota, M.; Ohashi, M.; Tsuji, F. I. *Proc. Natl. Acad. Sci. U.S.A.* **1996**, *93*, 13817.
(6) Stübner, M.; Schellenberg, P. *J. Phys. Chem. A* **2003**, *107*, 1246−1252.
(7) Webber, N. M.; Litvinenko, K. L.; Meech, S. R. *J. Phys. Chem. B* **2001**, *105*, 8036.
(8) Kummer, A. D.; Kompa, C.; Niwa, H.; Hirano, T.; Kojima, S.; Michel-Beyerle, M. E. *J. Phys. Chem. B* **2002**, *106*, 7554.
(9) Mandal, D.; Tahara, T.; Webber, N. M.; Meech, S. R. *Chem. Phys. Lett.* **2002**, *358*, 495−501.

10.1021/ja037278m CCC: $27.50

decays within 0.5 ps. The knowledge of the detailed photochemical mechanism underlying such ultrafast fluorescence decay would greatly enhance our chances to comprehend the fluorescence enhancement seen in GFP. In particular, although there are only limited gas-phase spectroscopic measurements of **2**,[10−12] it is apparent that the mapping of its excited-state potential energy surface in vacuo would provide a rigorous basis for the formulation of a mechanism consistent with the ultrafast nature of the fluorescence decay. This research target constitutes the major objective of the present work.

Recent studies[13] on different models of the retinal chromophore of rhodopsin proteins (a polyenal protonated Schiff base) suggest that the level of theory required for a correct description of the excited- and ground-state geometrical and electronic structure of the conjugated chromophores must include the treatment of electron dynamic correlation. In particular, the use of an ab initio CASPT2//CASSCF/6-31G* strategy (i.e., geometry optimization at the CASSCF level and energy evaluation at the CASPT2 level) on an 11-cis retinal chromophore model yields reasonable values for the backbone geometry absorption and emission λ_{max} and change in dipole moment ($\Delta\mu$) when compared with the solution data. Here, we show that the same strategy can be successfully used in a computational investigation of the intrinsic (i.e., in vacuo) excited-state relaxation path of **3**: a 2,3-demethyl model of the experimental system **2**. To our knowledge, this represents the highest level of theory applied to a realistic GFP fluorophore model so far. We will show that it is possible to establish: (i) the origin and molecular/electronic structure of **FS** and (ii) the nature of the fluorescence decay channel.

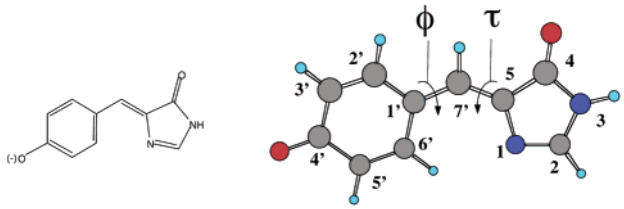

3

ϕ = C2'-C1'-C7'-C5

τ = C1'-C7'-C5-C4

Previous quantum chemical studies on the spectroscopy and excited-state relaxation of the GFP fluorophore model **3** have been carried out by the group of Rösch[14] and by Weber et al.[15] using different semiempirical levels of theory (i.e., AM1 CISD and OM2/PERTCI, respectively) and more recently by Laino et al.[16] that applied a semiempirical CAS-CI//DFT strategy to model **2**. The spectra of more complex models have also been investigated by Voityuk et al.[17] at the NDDO-G level and by Helms et al.[18] using post-SCF ab initio methods (CIS, MCSCF//MCQDPT) and by Das et al.[19] (SAC/SAC−CI). The excited-state evolution of **3** was investigated at the semiempirical level of theory through potential energy surface scans[14,15] where the ϕ and τ torsional coordinates describing the twisting about the $C_{1'}-C_{7'}$ and $C_{7'}-C_5$ ring-bridging bonds were kept at fixed values and the remaining coordinates optimized. In the contribution of Weber et al.,[15] the geometry optimization was carried out on the excited-state energy surface thus approaching a more realistic description of the excited-state relaxation. These authors not only investigated the coordinates driven by the single torsions (i.e., ϕ and τ) but also a coordinate defined by a simultaneous change of ϕ and τ to mimic the so-called "hula-twist" motion first proposed as a space-saving reaction coordinate for the isomerization of the retinal chromophore in the cavity of rhodopsin proteins.[20]

Scheme 1

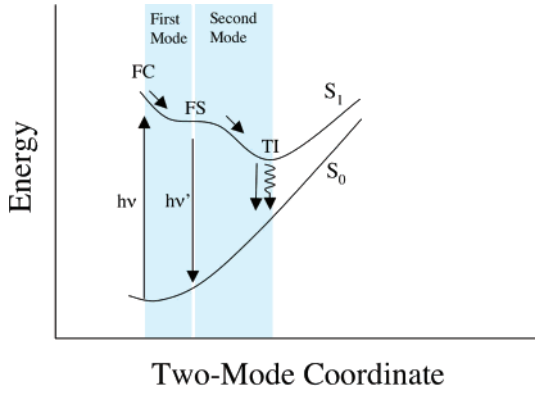

Despite the exploratory value of the computational work mentioned above, the detailed structure of the excited-state relaxation path of the anionic form of the GFP fluorophore remains unknown. In particular, since the excited-state geometry optimizations were limited to points with 0°, 90°, and 180° values of the ϕ and τ coordinates,[15] the structure of the reaction paths (and, most importantly, the presence of excited-state barriers) connecting planar (e.g., 0°) to 90° twisted structures were not documented. Furthermore, a description of the path controlling the relaxation following photon absorption (i.e., from the Franck−Condon point (**FC**)) was not provided. Finally, while it was suggested[15] that a surface touching may be reached along a hula-twist (HT) path such an energy surface touching or intersection has never been rigorously located and characterized for a GFP fluorophore model.

In the present work, the S_1 relaxation coordinate is *not* postulated. In fact, the mapping is carried out constructing the S_1 branch of the photochemical reaction path.[21] This is defined as the minimum energy path connecting **FC** to the possible $S_1 \rightarrow S_0$ radiationless deactivation channel in the full space of the 3N-6 vibrational degrees of freedom of the molecule (N is the number of atoms of the system). Notice that no starting hypothesis or geometrical constraint on the modes dominating the relaxation coordinate are required in this computation that is therefore unbiased. As we will show below, this strategy

(10) Andersen, L. H.; Lapierre, A.; Nielsen, S. B.; Pedersen, S. U.; Pedersen, U. V.; Tomita, S. *Eur. Phys. J.* **2002**, *F 20*, 597−600.
(11) Boyé, S.; Krogh, H.; Nielsen, I. B.; Nielsen, S. B.; Pedersen, S. U.; Pedersen, U. V.; Andersen, L. H. *Phys. Rev. Lett.* **2003**, *90*, 118103(118104).
(12) Nielsen, S. B.; Lapierre, A.; Andersen, J. U.; Pedersen, U. V.; Tomita, S.; Andersen, L. H. *Phys. Rev. Lett.* **2001**, *22*, 228102(228104).
(13) González-Luque, R.; Garavelli, M.; Bernardi, F.; Merchán, M.; Robb, M. A.; Olivucci, M. *Proc. Natl. Acad. Sci. U.S.A.* **2000**, *97*, 9379−9384.
(14) Voityuk, A. A.; Michel-Beyerle, M.-E.; Rosch, N. *Chem. Phys. Lett.* **1998**, *296*, 269.
(15) Weber, W.; Helms, V.; McCammon, J.; Langhoff, P. *Proc. Natl. Acad. Sci. U.S.A.* **1999**, *96*, 6177.
(16) Laino, T.; Nifosì, R.; Tozzini, V. *Chem. Phys.* **2004**, *298*, 17−28.
(17) Voityuk, A. A.; Kummer, A. D.; Michel-Beyerle, M.-E.; Rosch, N. *Chem. Phys.* **2001**, *269*, 83.
(18) Helms, V.; Winstead, C.; Langhoff, P. W. *J. Mol. Struct. (THEOCHEM)* **2000**, *506*, 179.
(19) Das, A. K.; Hasegawa, J.-Y.; Miyahara, T.; Ehara, M.; Nakatsuji, H. *J. Comput. Chem.* **2003**, *24*, 1421−1431.
(20) Liu, R. S. H. *Pure Appl. Chem.* **2002**, *74*, 1391−1396.
(21) Robb, M. A.; Garavelli, M.; Olivucci, M.; Bernardi, F. In *Reviews in Computational Chemistry*; Lipkowitz, K. B., Boyd, D. B., Eds.; Wiley-VCH: New York, 2000; Vol. 15, pp 87−146.

yields the mechanistic picture of Scheme 1. The most remarkable feature of such mechanism is that the fluorescence decay primarily occurs through the *barrierless* relaxation of the planar **FS** structure to a nonfluorescent 90° twisted intermediate (**TI1**) via torsional relaxation about the ϕ coordinate. While we show that, in principle, **TI1** could reach a HT conical intersection **CI** (that is rigorously determined via conical intersection optimization), the CASPT2 energy profile as well as the two-mode structure of the reaction coordinate suggest that this would be unlikely at both high and low temperatures.

2. Computational Methods

The molecular structures defining the excited-state reaction coordinates for the anion **3** have been obtained via minimum energy path (MEP) computations using the complete active space self-consistent field (CASSCF) level of theory with the 6-31G* basis set (as discussed below, the need for a more diffuse basis set has been assessed by running few 6-31+G* control computations) and an active space of 12 electrons in 11 π-orbitals (12e/11o). This is an incomplete π active space, given that the complete 16e/14o cannot presently be computationally handled. Accordingly, the nitrogen π-lone pair orbital (i.e., the lone-pair on N3) and the lowest and highest benzene valence π-orbitals (i.e., the lowest HOMO and highest LUMO) are excluded from the active space. A two-root (S_0, S_1) state-average procedure has been used to avoid CASSCF convergence problems in *all* excited-state calculations. The detailed procedure adopted to carry out the MEP computations is reported in refs 21 and 22. In all cases, progression along the MEP is given in mass-weighted Cartesians (au = $amu^{1/2}a_0$). Further investigation of the structure of the S_1 potential energy surfaces of **3** involved fully unconstrained geometry optimization of the ground-state equilibrium structure **FC**, three excited-state minima (**FS**, **TI1**, and **TI2**), and one conical intersection **CI** carried out at the same level of theory used for the MEP computations. (All computations have been carried out using the methodologies available in the GAUSSIAN98 series of programs.[22]) To improve the reaction path energy profile, we have performed single-point multiconfigurational second-order perturbation theory computations along a selected number of MEP points and all the stationary points by using the CASPT2 method[23] included in MOLCAS-5.[24] The zeroth order wave functions used in the CASPT2 calculation are two-root (S_0, S_1) and three-root (S_0, S_1, S_2 for **FS** only) state-average 12e/11o CASSCF wave functions. The qualitative change of the nature of the wave function is monitored by evaluating the charge distribution (Mulliken charges) along the backbones of **3** at the CASSCF level of theory. The effect of diffuse functions on the reaction paths has been assessed by running excited-state 6-31+G* computations for the optimized **FC**, **FS**, **TI1**, **TI2** energy minima and **CI** conical intersection structure. Comparison of the CASSCF/6-31G* and CASSCF/6-31+G* data shows that there is no relevant change in the relative energies (see Table 2 in the Supporting Information section for the CASSCF/ 6-31+G* data).

Table 1. Ground- and Excited-State CASPT2 Absolute Energies for the GFP Fluorophore Model **3**

structure	state	CASPT2 energy (au)	reference weight[a]
FC	S_0	−643.40237	0.62
	S_1	−643.30433	0.61
FS	S_0	−643.39948	0.62
		(−643.39980)	(0.62)
	S_1	−643.30965	0.61
		(−643.31002)	(0.61)
	S_2	(−643.26785)	(0.60)
TI1	S_0	−643.35504	0.62
	S_1	−643.32118	0.61
$TS_{FS\rightarrow TI2}$	S_0	−643.39004	0.62
	S_1	−643.30750	0.61
TI2	S_0	−643.34393	0.62
	S_1	−643.32380	0.61
CI	S_0	−643.30911	0.62
	S_1	−643.30181	0.61

[a] Weight of the CASSCF reference function (i.e., the zeroth order function) in the first-order function. Close values indicate that energy differences (e.g., barriers and excitation energies) can be correctly evaluated.

The simulation of the absorption spectra has been carried out by extracting, from the computed equilibrium structures of S_0 and S_1, the displacement parameters $B_{S0,S1}$ which govern the vibronic structure of the $S_0\rightarrow S_1$ electronic transition, as described, for instance, in ref 25. A Lorentzian line width of 100 cm^{-1} has been associated to each computed vibronic transition. Numerical frequency computations on **3** and **FS** have been carried out at the CASSCF/6-31G* level (see above) and showed no imaginary frequencies. The shallow CASSCF barriers found along the **FS→TI1** and **FS→TI2** paths (see Section 3.2 below) have not been located directly as the flatness of the S_1 energy surface makes transition-state optimization unpractical. Similarly, $\mathbf{TS_{FS\rightarrow TI2}}$ corresponds to the maximum along the CASPT2//CASSCF energy profile of **FS→TI2** as transition-state optimization is currently out of reach at this level of theory.

3. Results and Discussion

The CASPT2 energies of the energy minima, transition structure, and conical intersection discussed in the next subsections are collected in Table 1. These data can be used to validate the computational strategy defined in Section 2. First of all, the computed $S_0 \rightarrow S_1$ vertical excitation energy, corresponding to a λ_{max} value of 465 nm (see Figure 1a), compares well with the measured[10] 480-nm gas-phase λ_{max} of **2** (see Figure 1b). The predicted CASPT2//CASSCF λ_{max} seems to be improved with respect to the recent[19] SAC-CI//B3LYP value of 558 nm predicted for **2**. The corresponding oscillator strength (*f*) is 0.35 indicating that the $S_0\rightarrow S_1$ transition is a spectroscopic state for this species. Wave function analysis shows that the transition is dominated by a HOMO−LUMO single excitation between orbitals localized on the C1′−C7′−C5 bridge (in Scheme 2 we display the corresponding two-root state-average CASSCF orbitals).

The computed 465-nm λ_{max} also agrees with the λ_{max} of the GFP anionic (B) band obtained by deconvolution of the 77 K spectrum of GFP by the group of Boxer[4] (see Figure 1c). Furthermore, the simulation of the absorption in the 400−500-nm range compares reasonably well with the experimental B-spectrum[4] (compare Figure 1a and 1c). More specifically, considerable activity is computed for a mode at 1450 cm^{-1} that will be shown (see below) to correlate with the S_1 relaxation path. The computed activity in this frequency region agrees with

(22) Frisch, M. J.; Trucks, G. W.; Schlegel, H. B.; Scuseria, G. E.; Robb, M. A.; Cheeseman, J. R.; Zakrewski, V. G.; Montgomery, J. A., Jr.; Stratmann, R. E.; Burant, J. C.; Dapprich, S.; Millam, J. M.; Daniels, A. D.; Kudin, K. N.; Strain, M. C.; Farkas, O.; Tomasi, J.; Barone, V.; Cossi, M.; Cammi, R.; Mennucci, B.; Pomelli, C.; Adamo, C.; Clifford, S.; Ochterski, J.; Petersson, G. A.; Ayala, P. Y.; Cui, Q.; Morokuma, K.; Malick, D. K.; Rabuck, A. D.; Raghavachari, K.; Foresman, J. B.; Cioslowski, J.; Ortiz, J. V.; Stefanov, B. B.; Liu, G.; Liashenko, A.; Poiskorz, P.; MKomaromi, I.; Gomperts, R.; Martin, R. L.; Fox, D. J.; Keith, T.; Al-Laham, M. A.; Pen, C. Y.; Nanayakkara, A.; Gonzalez, C.; Challacombe, M.; Gill, P. M. W.; Johnson, B. G.; Chen, W.; Wong, M. W.; Andres, J. L.; Head-Gordon, M.; Replogle, E. S.; Pople, J. A. **1998**.
(23) Andersson, K.; Malmqvist, P.-A.; Roos, B. O. *J. Chem. Phys.* **1992**, *96*, 1218.
(24) Andersson, K.; Barysz, M.; Bernhardsson, A.; Blomberg, M. R. A.; Cooper, D. L.; Fülscher, M. P.; Graaf, C.; Hess, B. A.; Karlström, G.; Lindh, R.; Malmqvist, P.-A.; Nakajima, T.; Neogrády, P.; Olsen, J.; Roos, B. O.; Schimmelpfennin, B.; Schütz, M.; Seijo, L.; Serrano-Andrés, L.; Siegbahn, P. E. M.; Stålring, J.; Thorsteinsson, T.; Veryazov, V.; Widmark, P.-O. Lund University, Sweden, 2002.
(25) Negri, F.; Zgierski, M. Z. *J. Chem. Phys.* **1993**, *99*, 4318−4326.

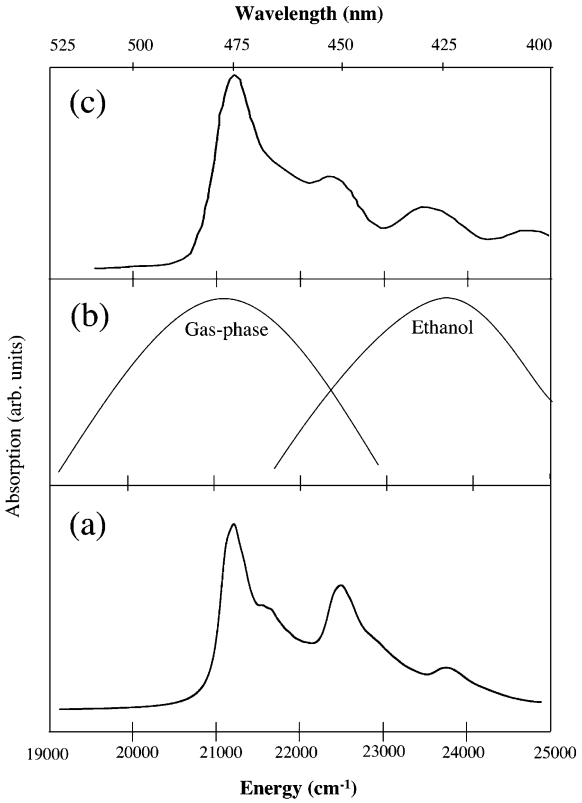

Figure 1. (a) Simulated (see Section 2) absorption spectrum of model **3**. (b) Unstructured experimental absorption spectra of model **2** in solution and in the gas phase. Spectra are adapted from ref 10. (c) Absorption spectrum of the anionic form of wild-type GFP obtained by deconvolution. Adapted from ref 26.

Scheme 2

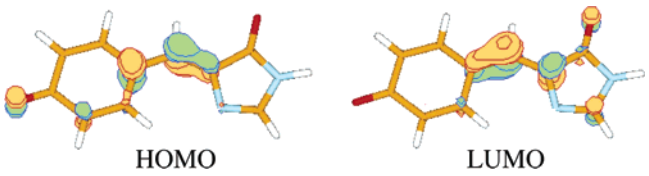

the band observed at 1510 cm^{-1} in absorption (see ref 29). The simulation also agrees with the absorption spectrum (not shown) of the S65T GFP mutant[26] containing an anionic chromophore. On the other hand, the computed gas-phase value for the change in dipole moment of model **3** is ca. 1 D (6.3 and 5.3 D for the S_0 and S_1 state, respectively) and therefore appears to be very different from the ca. 7 D value measured for GFP[4] (similarly, a SAC-CI//B3LYP calculation yields ca. 2 D change[19]).

The fact that the observed gas-phase λ_{max} value for **2**[10] and for GFP[26] are red-shifted with respect to the corresponding value for **2** in *n*-propanol solution[9] (see Figure 1b) suggests that, at **FC**, the protein environment is more similar to the gas-phase than to the solution environment. In other words, while in solution one has ca. 50-nm λ_{max} blue-shift with respect to the gas-phase (this is explained by the fact that the counterion and solvent molecules will be arranged in such a way to optimally stabilize the ground-state structure with respect to the excited-state structure), in the protein such a blue-shift is not observed. This effect is reminiscent of that recently documented[27] for the visual photoreceptor rhodopsin. In fact, while rhodopsin and its gas-phase retinal chromophore have close λ_{max} values, these are red-shifted with respect to the λ_{max} of the same chromophore in methanol solution. It has been computationally shown[27] that such effect is because the unique charge distribution of the protein counterbalances that of its own internal counterion.

The Mulliken S_1 and S_0 (in brackets) charges at **FC** (see Figure 2a) are consistent with a limited change in dipole moment. Indeed, the major change observed upon $\pi \rightarrow \pi^*$ excitation corresponds to a limited migration of the negative charge from the phenyl ring to the imidazole ring (see, for instance, the negative charge decrease at C3′ and the negative charge increase at N1 and N3). The total amount of charge translocation is of ca. 0.1 electrons (when "cutting" the structure at the C1′−C7′ bond) from the phenyl to the imidazole moiety.

3.1 Origin and Nature of the Fluorescent State. In Figure 3, we report the result of relaxation path computations starting from **FC**. It is apparent that it was possible to locate a single relaxation path that preserves the planarity of the system and ends at an S_1 stationary point **FS**. The relaxation occurs, exclusively, along a stretching coordinate ultimately dominated by the expansion of both the bridge bonds $C_{1'}-C_{7'}$ and $C_{7'}-C_5$ of ca. 0.05 Å and a reduction of the $C_{1'}-C_{7'}-C_5$ angle (from 133° to 128°). These changes are qualitatively consistent with those reported by Helms et al.[18] on the basis of a 2e/2o CASSCF computation on **3**. However, in such an approximate computation the bond lengths $C_{1'}-C_{7'}$ and $C_{7'}-C_5$ appear to be overestimated.

It is evident that the initial relaxation is preparatory with respect to facile twisting about the corresponding ϕ and τ torsions. The nature of the **FS** torsional flexibility has been investigated via vibrational frequency computations. The results confirm that **FS** corresponds to an extremely flat energy minimum featuring three <200 cm^{-1} frequencies. The first (unscaled) frequency (119 cm^{-1}) corresponds to the $C_{1'}-C_{7'}-C_5$ in-plane bending mode. The modes associated to the second (127 cm^{-1}) and third (158 cm^{-1}) (unscaled) frequencies are given in Scheme 3. It can be seen that these modes correspond to the out-of-plane deformations of the planar **FS** structure. In particular, the first mode appears to be a combination of the torsional angle τ with the pyramidalization at the C7′ centre. In contrast, the second mode seems to be completely dominated by the ϕ torsion. Clearly, such low-frequency modes confirm the idea that **FS** may undergo large amplitude deformations along ϕ and τ. The **FC** → **FS** energy profile of Figure 3 also suggests that in this region the S_1 energy surface is not harmonic. However, the central structure in Figure 3 indicates that the relaxation coordinate maintains the same character along the path. Since this relaxation direction correlates with a 1450 cm^{-1} vibrational mode of **FS** (see Scheme 3), this is the mode that must get impulsively populated upon **FC** relaxation.

At **FS** the predicted vertical S_0-S_1 energy gap (see Table 1) is consistent with an emission λ_{max} value of 507 nm. (This value appears to be considerably blue-shifted with respect to the SAC−CI//CIS computations for **2** yielding a value of 579 nm.[19]) The S_2 state is located 25 kcal mol^{-1} above S_1 indicating emission from a single electronic state. The computed value is

(26) Bublitz, G. U.; King, B. A.; Boxer, S. G. *J. Am. Chem. Soc.* **1998**, *120*, 9370−9371.
(27) Ferré, N.; Olivucci, M. *J. Am. Chem. Soc.* **2003**, *125*, 6868−6869.
(28) Morise, H.; Shimomura, O.; Johnson, F. H.; Winant, J. *Biochemistry* **1974**, *13*, 2656.
(29) Ward, W. W.; Cody, C. W.; Hart, R. C.; Cormier, M. J. *Photochem. Photobiol.* **1980**, *31*, 611.

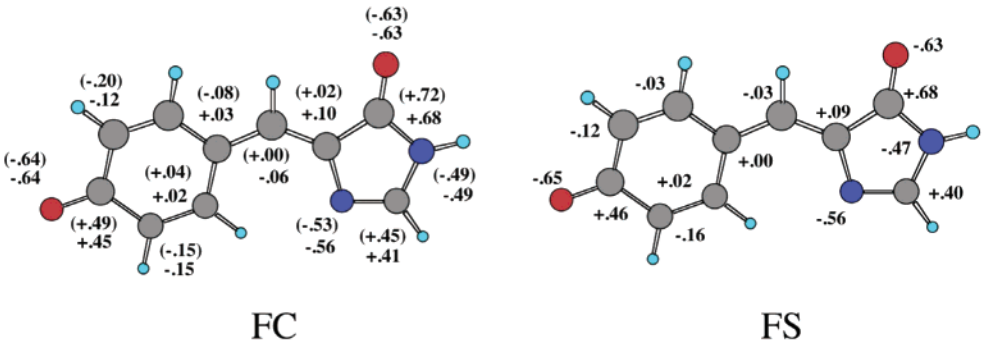

Figure 2. Mulliken charges (hydrogens summed on the corresponding heavy atoms) for the S_1 state of **FC** and **FS**. For **FC** the S_0 charges are also given (values in brackets).

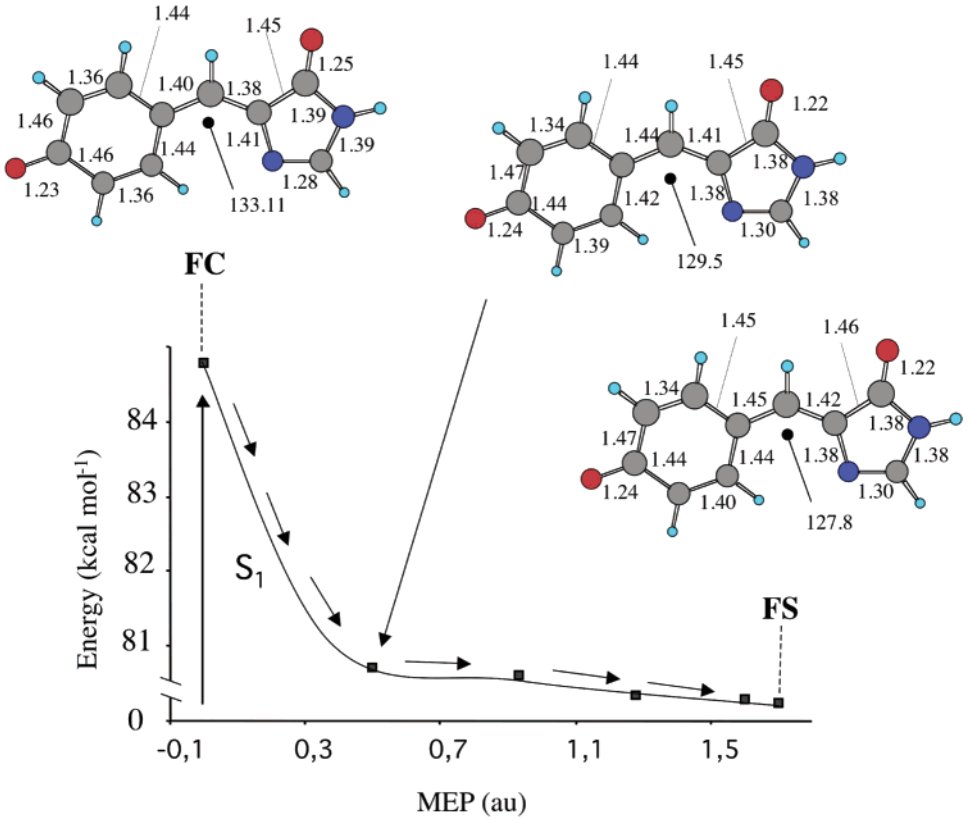

Figure 3. CASPT2 energy profile for the S_1 state along the computed S_1 **FC** → **FS** relaxation coordinate of the GFP chromophore model **3**. The structures (geometrical parameters in Å and degrees) document the progression of the molecule along the coordinate (in mass-weighted atomic units).

some 20−30 nm red-shifted with respect to the fluorescence λ_{max} measured in ethanol solution[7] probably because of counterion preferential ground-state stabilization. On the other hand, the computed λ_{max} value agrees remarkably well with the 508-nm λ_{max} value corresponding to the GFP green emission[28,29] thus indicating that the protein environment seems to be designed in such a way to mimic the gas-phase anion at least in the regions near **FC** and **FS**. This is reinforced by the 492-nm computed 0−0 adiabatic excitation of **3** that is only 15 nm red-shifted from the value observed[30] for the anionic form of the chromophore in GFP. These computational results strongly indicate that the planar structure **FS** represents the fluorescent state of the GFP chromophore. This conclusion is somehow further reinforced by the fact that the 1800 cm^{-1} Stokes shift, predicted on the basis of the data given in Table 1, compares well with the less than 2000 cm^{-1} Stokes shift observed[9] for **2** in *n*-propanol solution. The satisfactory agreement between the observed and computed fluorescence λ_{max}, 0−0 transition, and Stokes shift provides a further validation of the level of theory used in the present work.

The results of S_1 Mulliken charge analysis at **FS** is given in Figure 2. It is apparent that no substantial change in the position/distribution of the negative charge is observed upon **FC** → **FS** relaxation. This finding is consistent with the fact that **FS** has the same electronic nature of the vertically populated S_1 state. This same conclusion is supported by the computed **FC** → **FS** "horizontal" change in S_1 dipole moment that is ca. 0.1 D (see also Table 2 in the supporting info).

3.2 Decay of the Fluorescent State: the S_1 Twisted Intermediates. In Figure 4, we report the results of reaction/relaxation path computations starting at **FS**. Two different relaxation paths have been located that are dominated by the

(30) Creemers, T. M. H.; Lock, A. J.; Subramaniam, V.; Jovin, T. M.; Voelker, S. *Nat. Sruct. Biol.* **1999**, *6*, 557.

Scheme 3

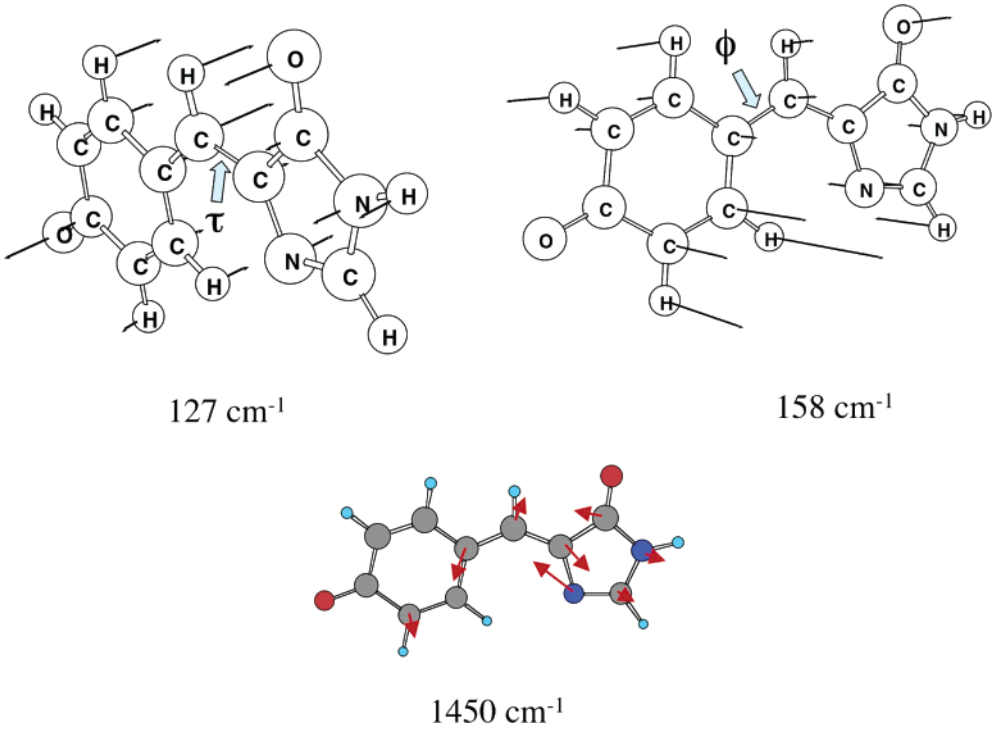

change of the torsional angles ϕ and τ, respectively. The shapes of the corresponding energy profiles are qualitatively consistent with those obtained on the basis of surface scans carried out at the semiempirical level of theory.[14,15] It is apparent from inspection of Figure 4 that while at the CASSCF level of theory two, previously undetected, small barriers restrain evolution along both relaxation paths; at the superior CASPT2 level one of these barriers is reduced and the other is augmented indicating that the excited-state evolution of **FS** is strongly biased toward the path dominated by the ϕ torsion. Relaxation along this path leads to the 90° twisted S_1 intermediate **TI1** (an S_1 energy minimum). The fact that we could not determine a finite barrier along this path indicates that, at the CASPT2 level, **FS** does not correspond anymore to an energy minimum. However, as we will better discuss in section 3.4, the flatness of the S_1 energy profile in the **FS** region, suggests that this point can be described as a metastable species whose lifetime should be mainly controlled by the rate of internal vibrational energy redistribution (IVR) or by a <1 kcal mol^{-1} energy barrier (i.e., the expected accuracy of our CASPT2 energy profile). The alternative path characterized by torsional deformation about the τ coordinate leads to production of the different 90° **TI2** twisted species (a

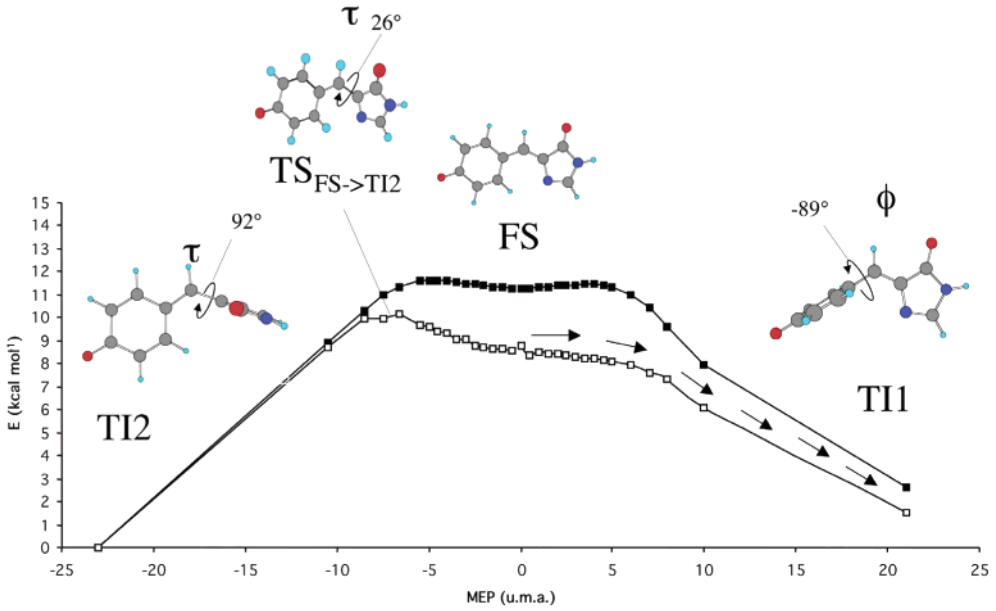

Figure 4. CASSCF (full squares) and CASPT2 (open squares) energy profiles for the electronic S_1 state along the computed **FS→TI1** (right) and **FS → TI2** (left) S_1 relaxation coordinates. $\mathbf{TS_{FS\rightarrow TI2}}$ indicates the transition structure controlling access to **TI2**. The stream of arrows indicates the energetically favored relaxation path. A change in shape of the reaction energy profiles after dynamic electron correlation correction (e.g., passing from CASSCF to CASPT2) has also been documented in other systems. See, for instance, a discussion in Sinicropi et al. *J. Am. Chem. Soc.* **2003**, *125*, 10947−10959.

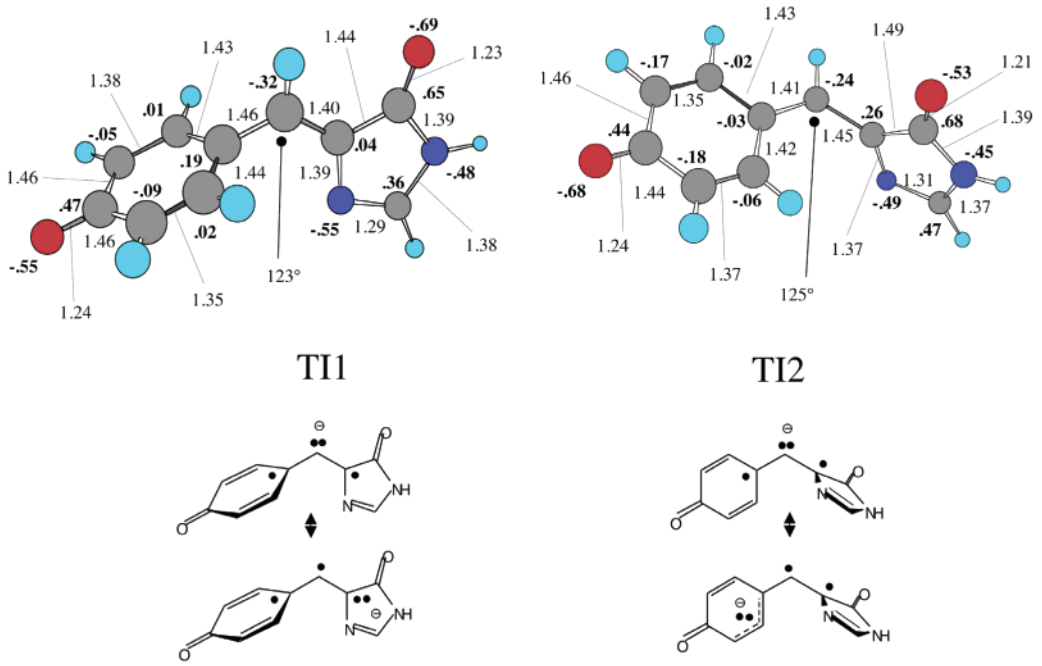

Figure 5. Geometrical and electronic structures of the S_1 intermediates **TI1** and **TI2**. The geometrical parameters (plain text) are given in Å and degrees. The wave function is qualitatively characterized in terms of the distribution of Mulliken charges (bold). The resonance structures consistent with the computed charge distribution are also given.

Scheme 4

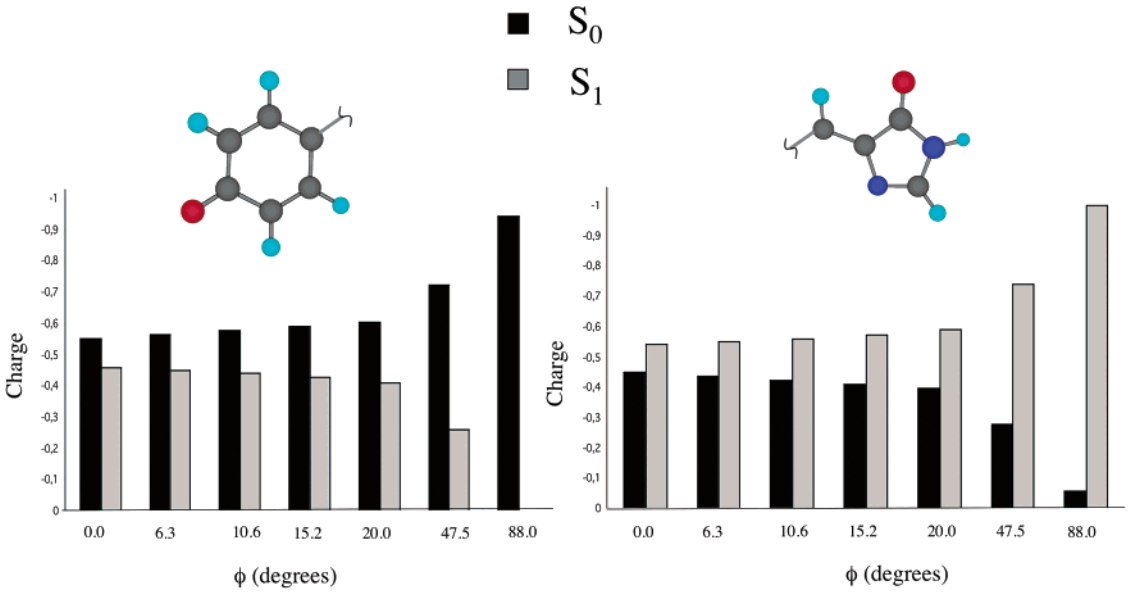

second S_1 energy minimum) that is ca. 2.5 kcal mol^{-1} more stable that **TI1**. However, the CASPT2 energy profile indicates that this path shall be less efficiently populated because of a 2 kcal mol^{-1} barrier controlling access to it. The difference between the CASSCF and CASPT2 energy profiles demonstrates that inclusion of the dynamic correlation energy correction is mandatory for the description of the excited-state reaction paths in **3**. Such correction changes the local topography of the **FS** region increasing the barrier along the τ torsion and eliminating that along the ϕ torsion. While an interpretation of this effect will be given below, we stress here that such change in topography is mechanistically important as, even in terms of a simple Arrhenius model, a barrier >1 kcal mol^{-1} would be inconsistent with a subpicosecond fluorescence lifetime.

Despite several attempts, no reaction path could be located along a hula-twist deformation where both the ϕ and τ torsions are changed simultaneously. Consistently with the suggestion of Weber et al.,[14,15] the results of a surface scan (not a reaction path!) along this coordinate demonstrates that along such deformation the S_1 energy slowly, but constantly, increases to a structure where the two rings are strongly twisted with respect to the original molecular plane and where the S_0–S_1 energy gap is zero. This structure (a conical intersection between the S_1 and S_0 states) located 5 kcal mol^{-1} above **FS** will be rigorously characterized in subsection 3.3.

The relaxation paths reported in Figure 4 suggest that **TI1** (and, to a lesser extent, **TI2**) represents the structure that will ultimately be populated upon excited-state relaxation and decay

Scheme 5

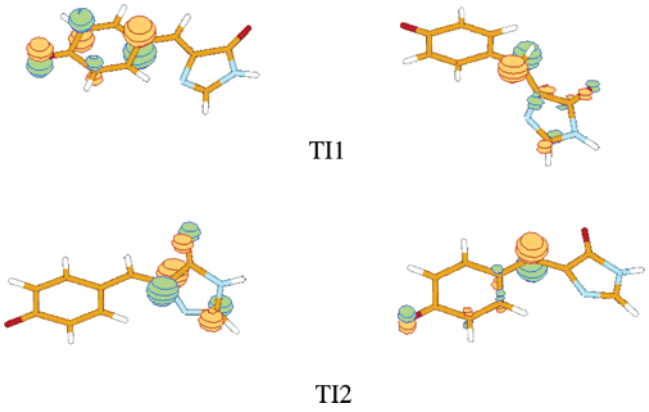

of the fluorescent state **FS**. Thus, the knowledge of the geometrical and electronic structure of the twisted intermediates is of fundamental interest. In Figure 5, we report the structural parameters of **TI1** and **TI2**. For **TI1**, clearly, the twisting deformation is accompanied by an extended change in bond orders. A qualitative analysis in terms of resonance structures suggests that such change must occur in correspondence to a charge translocation from the phenyl to the imidazole ring. This hypothesis is confirmed by the result of the analysis of the Mulliken charges along the computed **FS** → **TS1** isomerization path of Scheme 4.

At **TI1**, the S_1 charge is almost completely located on the imidazole moiety. More specifically, the negative charge resides on the C7′ (ca. 45%) and the imidazole ring (ca. 55%). Thus, the resonance formulas that appear to contribute to the electronic structure of **TI1** are the one reported in Figure 5. Notice that, consistently with these formulas, the twisted intermediate must have diradical character. In particular, the phenyl moiety must have a radical character while the imidazole moiety is a radical anion. The singly occupied orbitals of **TI1** are given in Scheme 5 (where we display the corresponding two-root state-average CASSCF orbitals) and are consistent with the resonance formula of Figure 5. Similar resonance formulas appear to determine the electronic structure of the alternative **TI2** intermediate. In fact, again, **TI2** displays a large change in charge distribution with respect to **FS**. A considerable portion of the negative charge is found on the bridge carbon atom C7′(ca. 25%). The remaining charge is instead located on the phenyl moiety (75%). The large charge redistribution in **TI1** and **TI2** is consistent with the values of the computed S_1 dipole moments that are 11 and 9 D, respectively, and much larger than the one computed for **FC** and **FS**. Furthermore, the same change suggests a large sensitivity of the **FS** → **TI1** and **FS** → **TI2** paths to solvent effects and, as we will better discuss below, to the protein environment.

It is apparent from comparison of the CASSCF and CASPT2 energy profiles seen in Figure 4 that the dynamic correlation energy correction leads to a preferential stabilization of the ϕ driven **FS** → **TI1** path. This is also reflected by the CASPT2 reduced energy difference between the **TI1** and **TI2** minima. The above charge analysis indicates that the dynamic correlation energy correction becomes larger when the negative charge is confined in the heterocyclic ring.

Similar to **FS**, the **TI1** and **TI2** S_1 energy minima may deactivate via emission. However, such emission should occur at a much longer wavelength. In particular, according to the data in Table 1, we predict an infrared emission λ_{max} at 958 nm

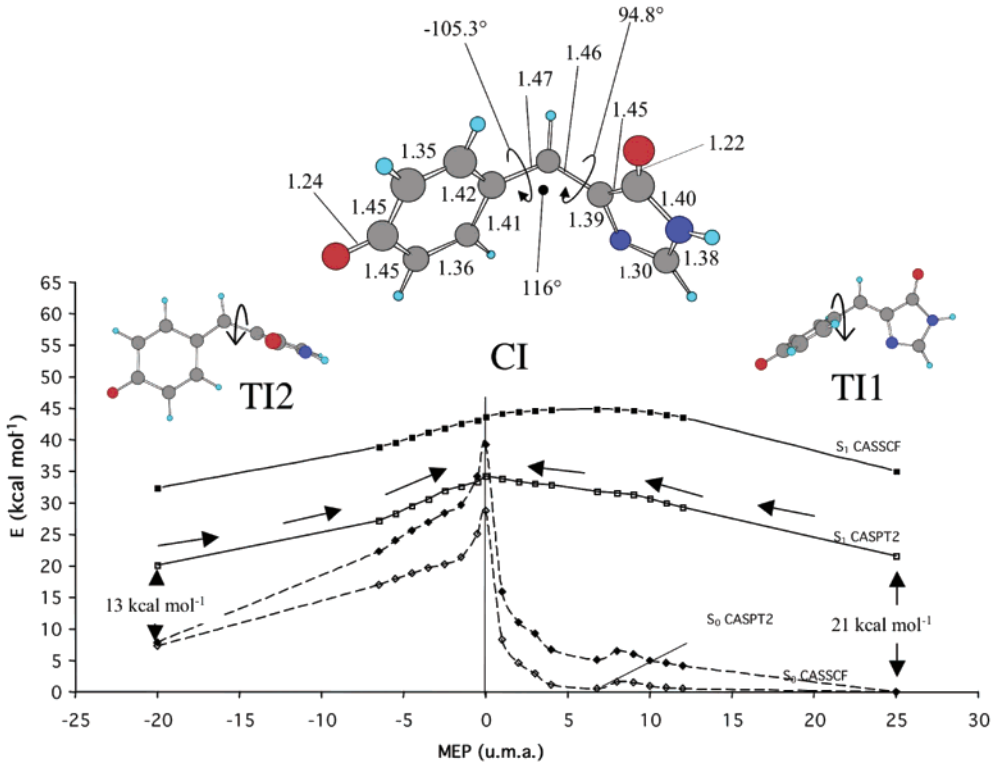

Figure 6. S_0 (diamonds) and S_1 (squares) CASSCF and CASPT2 energy profiles reported along the computed **CI** → **TI1** (right) and **CI** → **TI2** (left) S_1 relaxation coordinates. $\mathbf{TS_{FS\rightarrow TI2}}$ indicates the transition structure controlling access to **TI2**. The geometrical parameters relative to **CI** are given in Å and degrees. The stream of arrows indicates the energetically favored uphill paths from the intermediates to **CI**. The ca. 6 kcal mol^{-1} (S_0–S_1) energy gap at **CI** is explained by the limited efficiency of the available optimization method to locate sloped conical intersections.

Scheme 6

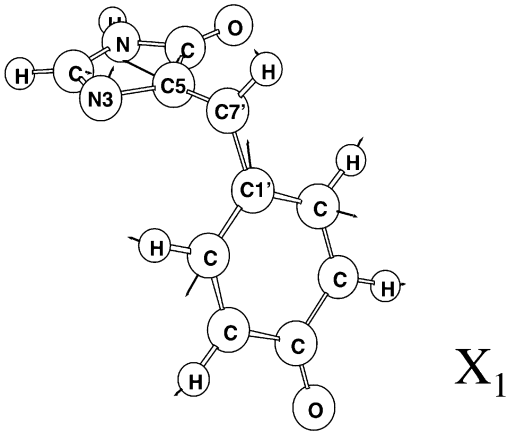

X_1

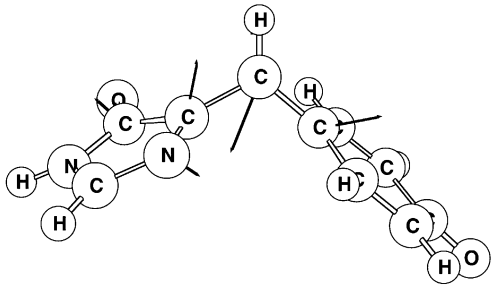

X_2

for **TI1**. At **TI2**, the S_0-S_1 energy gap is even smaller (12 kcal mol^{-1}) corresponding to an infrared emission of 2234 nm. The limited energy gap also suggests the possibility of an efficient internal conversion or the presence of a nearby S_0/S_1 conical intersection (see also subsection 3.4). Most likely because of its sloped topology, such intersection could not be located with the available computational tools. Thus, if it exists, its computation will constitute a major effort. (Recently, a twisted energy minimum of the "**TI2** type" and a nearby conical intersection characterized by a large pyramidalization at C_5 have been reported[31] for the *neutral form* of the chromophore model **3.**) Decay near **TI2** will lead to production of the Z/E stereoisomer of **3** while decay near **TI1** would lead to a degenerate conformational change that does not alter the structure of the initial material.

3.3 Nature of the Hula-Twist Conical Intersection. Previous studies[15] suggested that model **3** displays a potential energy surface touching or conical intersection associated with a space-saving hula-twist type conformation. While a surface scan indicated[15] that such structure is located too high in energy for playing a role in the fluorescence decay of the gas-phase fluorophore, it was suggested that the protein environment of certain GFP mutants could lead to a stabilization of such structure. Qualitative considerations also suggest that an S_1/S_0 HT conical intersection could provide a mechanistic explanation of the fluorescence decay observed in a confined environment (i.e., in a cold matrix) and of the reported[9] low sensitivity of the fluorescence decay rate to solvent viscosity. For this reason, we have searched a S_1/S_0 conical intersection and investigated its relationship with the **FS**, **TI1**, and **TI2** minima via relaxation path computations. The optimized **CI** structure has indeed the structural features characterizing a hula-twist type deformation. In fact, as documented in Figure 6, **CI** is characterized by highly twisted and expanded (larger than 1.45 Å) C1′−C7′ and C7′−C5 bonds. However, as we shall now discuss, relaxation out of the intersection is dominated by stretching deformations with no components along the two critical ϕ and τ twisting angles.

As mentioned above, no direct path connecting **FS** to **CI** could be located. However, as reported in Figure 6, we have located two paths describing the evolution of **TI1** and **TI2** toward **CI**. By inspection of such paths and of Table 1, one

Scheme 7

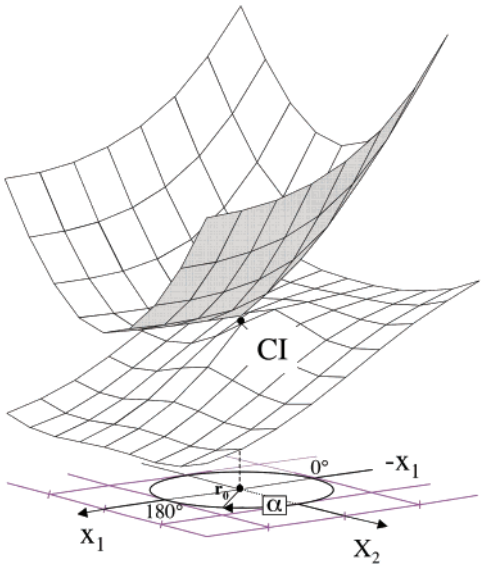

can see that the **CI** lies ca. 13 kcal mol^{-1} above **TI1** (i.e., ca. 5 kcal mol^{-1} above **FS**) and ca. 4 kcal mol^{-1} above $\mathbf{TS_{FS\rightarrow TI2}}$. This means that, according to the computed energies, **TI1** would evolve more efficiently along the **TI1** → **FS** → **TI2** path rather than toward the **TI1** → **CI** path.

To better clarify the nature of this conical intersection, we have investigated the shape and electronic structure of the S_1 and S_0 potential energy surfaces in the vicinity of **CI**. This is done by plotting the S_0 and S_1 energies and S_1 charges along a circular cross section centered on the **CI** and lying on the "branching plane". Such plane contains the molecular deformations that split the S_1/S_0 degeneracy and it is defined by the vectors $\mathbf{x_1}$ and $\mathbf{x_2}$ of Scheme 6 (the derivative coupling and gradient difference and of the S_1 and S_0 states, respectively; for convenience, here $\mathbf{x_2}$ indicates the gradient difference vector Schmidt orthogonalized to the derivative coupling vector $\mathbf{x_1}$). The first vector ($\mathbf{x_1}$) is dominated by a simultaneous stretching expansion of the C1′−C7′ bond and of the C5−N3 bond. The second vector ($\mathbf{x_2}$) is dominated by a bending of the C1′−C7′−C5 angle defining the shape of the bridge coupled with contraction of the C4−C5 bond and expansion of the C1′−C2′ bond. The hula-twist motion (i.e., either a conrotatory or disrotatory simultaneous change of the ϕ and τ angles) does not belong to the branching space and therefore will not lift the

(31) Toniolo, A.; Granucci, G.; Martinez, J. T. *J. Phys. Chem. A* **2003**, *107*, 3822−3830.

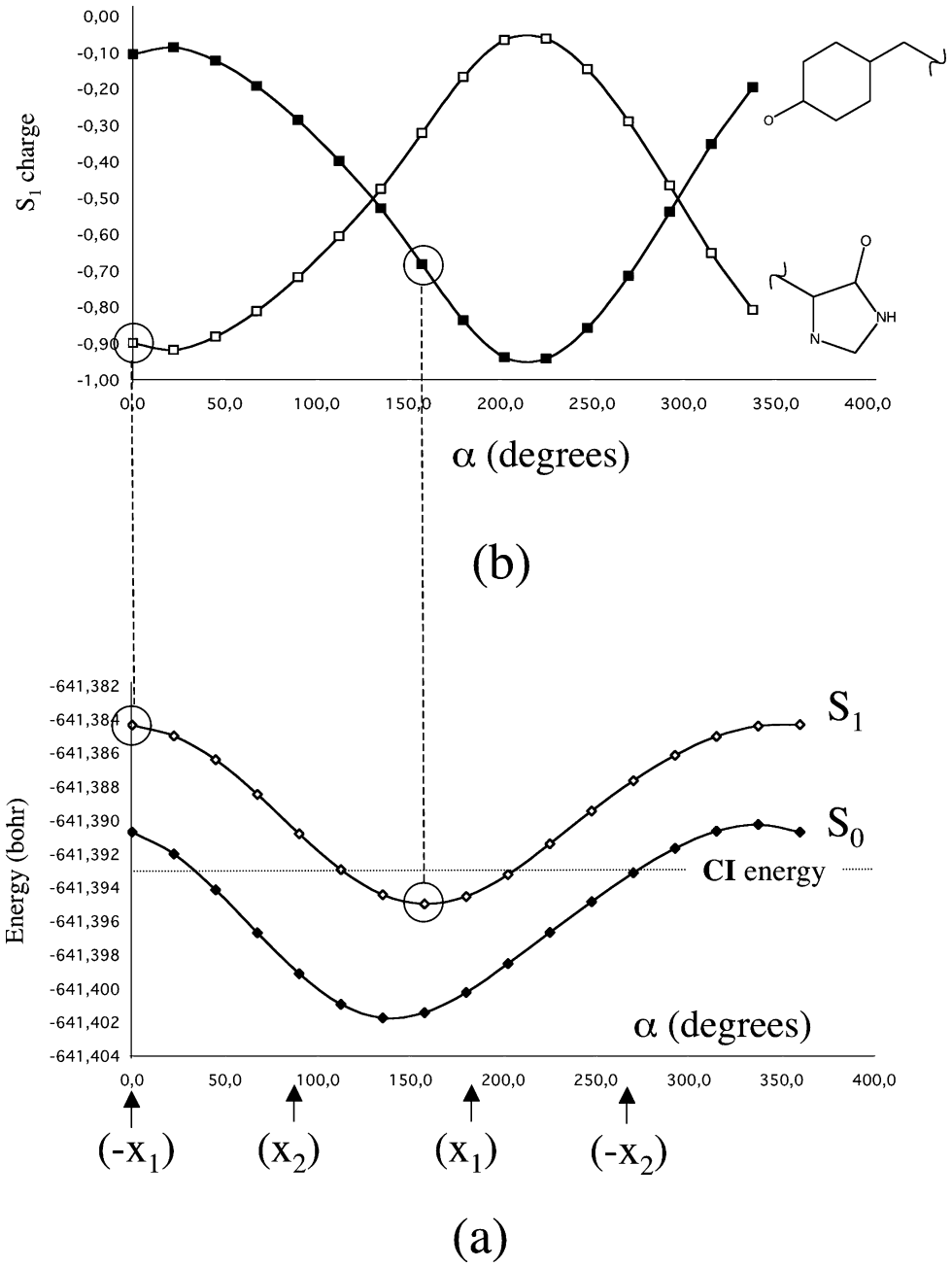

Figure 7. (a) S_0 (full diamonds) and S_1 (open diamonds) CASSCF energy profiles along a circular cross section of radius 0.2 au centered at **CI**. The angle α is defined in Scheme 7. (b) S_1 wave function analysis along the same circular cross section. The full squares indicate the total Mulliken charge on a convenient "phenyl moiety" (top structure). The open squares indicate the charges on the complementary "imidazole moiety" (bottom structure).

degeneracy (i.e., this motion belongs, locally, to the 3N-8 dimensional intersection space).

The chosen circular cross section—defined by a small 0.2 au radius ($\mathbf{r_0}$)—is schematically illustrated in Scheme 7. The result of a S_0 and S_1 CASSCF energy scan along this cross section is given in Figure 7a. The similarity of the S_1 and S_0 energy profiles and the presence of a single minimum and a single maximum opposite to it (i.e., displaced of ca. 180° along the circular cross section) suggest that the conical intersection topography corresponds to that of a sloped conical intersection consistent with that of Scheme 7. The direction of the slope, roughly pointing along $\mathbf{x_1}$, corresponds to a stretching deformation of the bridge bonds of the **CI** structure. In the downhill direction (i.e., at α ca. 0°), this deformation leads toward values of the stretching coordinates closer to the one of **FS**. Despite the lack of ϕ, τ torsional components, this relaxation must correspond to an initial downhill direction common to both the **TI1** → **CI** and **TI2** → **CI** paths of Figure 6.

In Figure 7b, we analyze the change in character of the wave function along the same loop by plotting the charge distribution relative to two moieties of **3**. It is evident from the plot that **CI** is a conical intersection between two electronic states related by an intramolecular charge transfer. In fact, along the loop the negative charge changes position by moving from one moiety to the other and returns, after 360°, to the original state. Along the S_1 relaxation direction ($\mathbf{x_1}$), the character of the charge transfer is mixed as 70% of the negative charge is located on the imidazole ring and the remaining part is located on the

Scheme 8

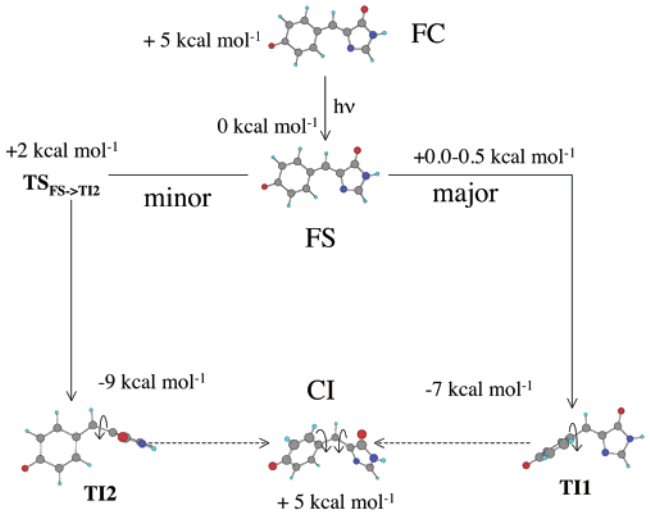

Scheme 9

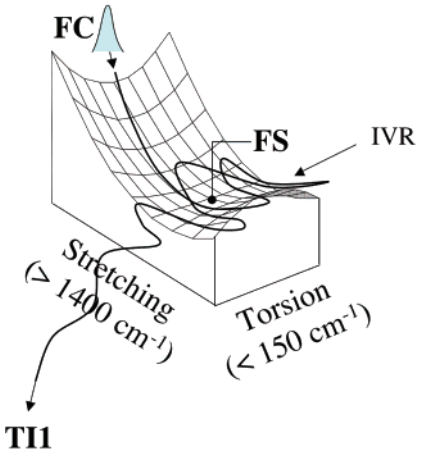

phenyl residue (the C7′ bridge carbon is substantially neutral for all structures along the circle). This mixed character suggests that the charge separation leading to the charge distribution seen in **TI1** and **TI2** will occur only after relaxation far from the **CI** region.

3.4 Comparison with the Experimental Data. In this section, the intrinsic fluorescence rise and decay mechanism determined for **3** is used in an attempt to rationalize the available time-resolved spectroscopic data for fluorophore **2** in solution. In Scheme 8, we summarize the results of our reaction path computations. It is apparent that, consistently with Scheme 1, the **FC**→**FS**→**TI1** path is the only path characterized by a barrierless (or nearly barrierless) relaxation. Since **FS** is the source of fluorescence, such path is tentatively assigned to the major fluorescence decay channel observed for **2**.

Since the **FC** → **FS** → **TI1** path is, effectively, bimodal the structure of this path is consistent with the two-state two-mode reaction path model[13] proposed to describe the photoisomerization of the retinal chromophore of rhodopsin proteins. Indeed, the **FC** → **FS** process occurs along a totally symmetric stretching mode (see Figure 3) that is uncoupled to the nontotally symmetric torsional mode describing the **FS** → **TI1** relaxation (see Figure 4).

In Scheme 9, we report a two-dimensional representation of the structure of the S_1 energy surface in the **FC** → **FS** region

Scheme 10

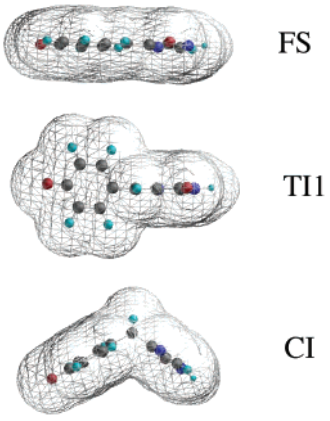

that can be used to discuss the wave packet dynamics starting at **FC**. Accordingly, after photoexcitation the wave packet undergoes relaxation to **FS**. As mentioned above, this relaxation correlates with a high-frequency stretching mode (ca. 1450 cm^{-1}) and thus must be fast (less than 50 fs as found for the retinal chromophore). At **FS** partial IVR from the initially populated mode to the low frequency (less than 200 cm^{-1}) torsional modes will prompt evolution toward the low-lying and nonfluorescent **TI1** intermediate.

Time-resolved fluorescence spectroscopy measurements[9] on **2** fail to detect a signal rise time at any probed wavelengths (475, 520, and 580 nm) but invariably detect a subpicosecond time scale (0.35−0.45 ps in methanol, *n*-proponal, and *n*-decanol solution) corresponding to the dominant fluorescence decay channel. These findings are fully consistent with the energy surface of Scheme 9. In other words, the fluorescence rise time must be faster than the fluorescence decay time that is determined by the IVR rate from the initially populated stretching mode to the torsional mode (or, possibly, controlled by a <1 kcal mol^{-1} barrier). Presently, the experimental fact[9] that an additional picosecond fluorescence decay channel is superimposed to the major subpicosecond decay channel (i.e., the fluorescence decay is described by a biexponential rather than monoexponential dynamics) cannot be unambiguously assigned. In fact, the S_1 potential energy structure described in Figure 4 and Scheme 9 suggests two different rationalizations. The first is that, at **FS**, IVR may result in the population of both the **FS** → **TI1** and **FS** → **TI2** competitive channels. This interpretation is consistent with the fact that at **FS** (i.e., locally) the vibrational modes dominated by the ϕ and τ torsional angles have similar frequencies. On the other hand, population of the barrier controlled **FS** → **TI2** path requires the presence of a non-negligible amount of excess vibrational energy along the torsional modes. While quantum or semiclassical dynamics calculations could, potentially, provide an answer to this issue, our structural (i.e., nondynamical) investigation cannot assess if enough excess energy will be available along such modes in the experimental conditions. The second, but less intuitive, explanation is based on the highly anharmonic topography of the S_1 energy surface. In fact, on such energy surface the relaxation dynamics can be complex leading to a splitting of the wave packet in two parts (i.e., classically, in two families of trajectories). The first part would decay within few oscillations (i.e., almost impulsively) leading to the shorter time scale, while the second part would remain in the **FS** region for a longer

Scheme 11

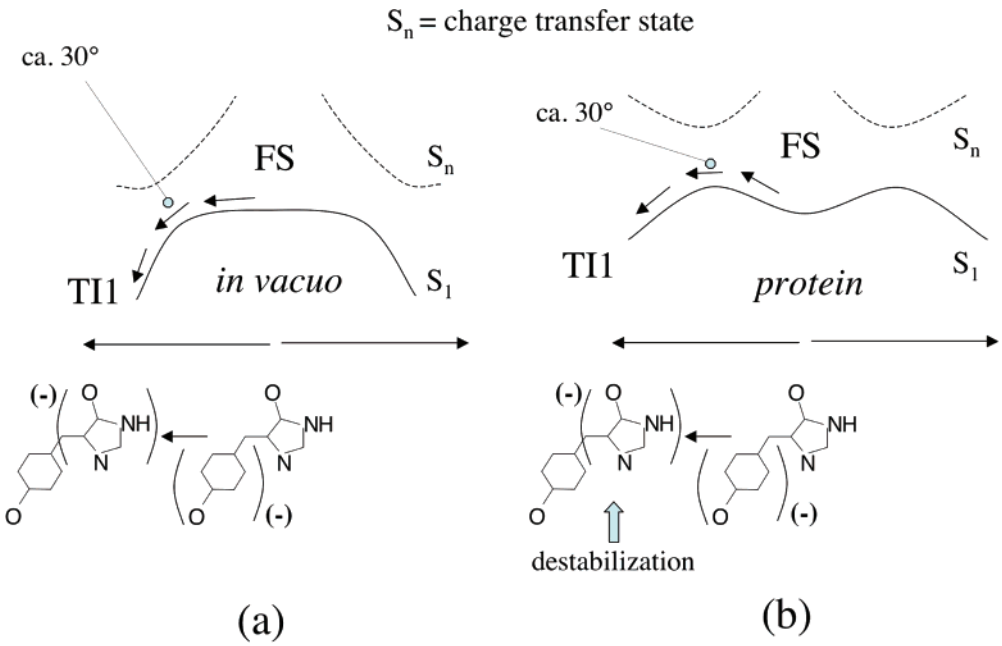

time. Computational evidences in favor of this second type of rationalization have been recently reported[32] for the case of the S_1 dynamics of a retinal chromophore on an energy surface very similar to that of Scheme 9.

The group of Meech used time-resolved polarization spectroscopy to investigate the ground-state recovery of **2** in three different solvents (methanol, ethanol, and butanol). These authors established that the recovery occurs with a dominant ca. 2 ps time constant thus setting an upper limit on the lifetime of a possible nonfluorescent S_1 intermediate. While the investigation of the detailed mechanism of the $S_1 \rightarrow S_0$ ultrafast decay of **3** goes beyond the scope of the present contribution, (this will be a matter of future research work in our laboratory), our computations indicate that the "dark" intermediate **TI1** is the primary product of the subpicosecond fluorescence decay. In contrast with $S_1 \rightarrow S_0$ decay at **TI2** or **CI**, the decay at **TI1** is consistent with regeneration of the starting Z-stereoisomer of **3** (i.e., the one investigated above) with no photochemical production of the alternative E-stereoisomer. This conclusion is consistent with the apparent lack of photochemistry observed for **2**.

The fluorescence decay studies mentioned above have been carried out in a range of solvents of different viscosity. It has been shown that both the shorter and longer fluorescence decay times are only weakly sensitive to viscosity. This fact is often taken as an indication that the decay of **FS** must involve a space-saving molecular deformation such as the one consistent with hula-twist motion. However, a qualitative inspection of a molecular model of **2** (or **3**) demonstrates that the **FS** → **TI1** motion does not require a dramatic change in molecular shape. This is illustrated above where we compare the geometrical deformation associated to this motion (i.e., a simple rotation of the phenyl group about its C1′−C7′ axis) and the rotation associated to the well-known viscosity sensitive E → Z isomerization of stilbene.[33] Regarding the idea that the hula-twist motion would provide a volume conserving path for the torsional deformantion of **FS**, in Scheme 10 we show that this may not be the case for **3**. Indeed, even a qualitative solvent accessible surface inspection for **TI1** and for the HT **CI** seems to support the idea of comparable geometrical changes.

(32) Cembran, A.; Bernardi, F.; Olivucci, M.; Garavelli, M., in press.

4. Conclusions

The results presented above establish the structure of the intrinsic excited-state relaxation path of the anionic form of the GFP fluorophore. In partial agreement with previous computations,[15] our CASPT2//CASSCF relaxation paths indicate that **FS** is a metastable planar species that, mainly, decays by barrierless torsional deformation of the phenyl single bond (i.e., through a photoinduced degenerate conformational change rather then through a Z/E isomerization). The alternative Z/E isomerization path leading to **TI2** is predicted to be less efficient as ca. 2 kcal mol^{-1} barrier restrains evolution of **FS** in that direction. The involvement of hula-twist deformation in the fluorescence decay can be excluded. Indeed, considering the short lifetime of **FS**, the probability that a significant fraction of the fluorescent population would acquire momentum along an uphill conrotatory or disrotatory hula-twist coordinate appears to be negligible.

Although the computed mechanism is strictly valid for the GFP fluorophore in vacuo, its two-state two-mode character is remarkably consistent with the ultrafast fluorescence rise and decay observed for the GFP anionic chromophore model **2** in solution. Furthermore, while the interaction with the solvent and counterion may change the energy profiles seen in Figure 5 and, possibly, the preference for evolution toward **TI1** (e.g., in ref 32 a remarkable solvent stabilization of a TI2-like conical intersection has been demonstrated for the neutral form of **3**), the apparent lack of photochemistry and the low sensitivity to solvent viscosity suggests that the determined mechanism remains valid.

The spectral similarities between the anionic GFP fluorophore and **2** (or our computational model **3**), suggest that a novel

(33) Waldeck, D. H. In *Conformational Analysis of Molecules in Excited States*; Waluk, J., Ed.; Wiley-VCH: 2000; pp 113−176.

mechanism may contribute to restrain the **FS → TI1** deformation in wild-type GFP. This mechanism, based on an excited-state destabilization of the negative charge on the imidazole ring, can be inferred by inspection of the bar diagram in Scheme 4. As shown in this scheme, at ca. 30° torsional deformation the S_1 charge distribution along the fluorophore backbone changes dramatically leading to a rapid shift of the negative charge from the phenyl ring toward the imidazole ring. Indeed, at **TI1** substantially all the negative charge is on the imidazole fragment. This qualitative change in charge distribution can be explained through the existence of an avoided crossing between S_1 and a charge transfer state S_n as illustrated in Scheme 11a. Destabilization of the S_n state or, in other words, destabilization of the negative charge in the imidazole unit leads to the diagram of Scheme 11b where an energy barrier is found at ca. 30° torsion along the energy profile. A demonstration of a possible excited-state destabilization effect of the complex GFP protein cavity requires state-of-the-art quantum mechanics/molecular mechanics computations that go beyond the scope of the present work. However, while steric interactions may contribute to the restrain force, **FS→TI1** represents a limited geometrical change in a situation where the orientation of the imidazole unit with respect to the protein cavity is fixed by two covalent bonds. More specifically, this only involves a partial rotation of the phenyl ring about the C7′−C4′ axis with a remarkable conservation of the hydrogen bond at the phenolic oxygen group. This conservation seems unlikely for motions characterized by the computed **FS→TI2** or hypothetic **FS→CI** coordinates.

Acknowledgment. Funds have been provided by the Università di Siena (Progetto di Ateneo 02/04) and HFSP (RG 0229/2000-M). E.M.N. is grateful for a grant provided by the Ministerio de Educación, Cultura y Deporte of Spain and Junta de Extremadura (Proyecto 2PR01A006). We thank CINECA for granted calculation time.

Supporting Information Available: Five pages containing (a) the Cartesian coordinates of the structures discussed in the text, (b) two tables containing the CASSCF/6-31+G* (Table 2) and CASSCF/ 6-31G* (Table 3) energies and corresponding dipole moments of the same structures, and (c) one table (Table 4) containing all S_0, S_1 and S_2 CASSCF/6-31G* energies. This material is available free of charge via the Internet at http://pubs.acs.org.

JA037278M